Frustrated antiferromagnetic honeycomb-tunnel-like lattice $CuR_2Ge_2O_8$ (R = Pr, Nd, Sm, and Eu)

Hwanbeom Cho,[1,2] Marie Kratochvílová,[1,2] Nahyun Lee,[1] Hasung Sim,[1,2] and Je-Geun Park[1,2,*]
[1]*Center for Correlated Electron Systems, Institute for Basic Science (IBS), Seoul 08826, Republic of Korea*
[2]*Department of Physics and Astronomy, Seoul National University, Seoul 08826, Republic of Korea*
(Received 7 October 2017; revised manuscript received 23 November 2017; published 22 December 2017)

New frustrated antiferromagnetic compounds $CuR_2Ge_2O_8$ (R = Pr, Nd, Sm, Eu) have been investigated using high-resolution x-ray diffraction, magnetic, and heat capacity measurements. These systems show different magnetic lattices depending on rare-earth element. The nonmagnetic Eu compound is a $S = 1/2$ two-dimensional triangular antiferromagnetic lattice oriented in the ac plane with geometrical frustration. On the other hand, the Pr, Nd, and Sm compounds show a three-dimensional honeycomb-tunnel-like lattice made of R^{3+} running along the a axis with the characteristic behavior of frustrated antiferromagnets.

DOI: 10.1103/PhysRevB.96.224427

I. INTRODUCTION

Geometrical frustration in magnetic materials has attributed significant attention over the last few decades, the origin of which is competing interactions due to the intrinsic geometrical configurations like triangular antiferromagnets (geometrical frustration) [1,2]. The other interactions such as further-nearest neighbor interaction in J_1-J_2 systems [3,4], Dzyaloshinskii-Moriya interaction [5–7], and single-ion anisotropy [8,9] can also play a role.

Frustration naturally leads to degenerate ground states that are the source of unusual physical phenomena. For example, a spin ice state emerges in pyrochlore system $Dy_2Ti_2O_7$ [8] due to the degeneracy of ground states with the two-in/two-out spin configuration in a tetrahedral lattice. For Heisenberg triangular antiferromagnets, the ground state has a 120° spin structure, which is infinitely degenerate due to the SO(3) symmetry [10]. As demonstrated many times in the field [8,11–14], finding a new frustrated system is an essential step that leads to discoveries of novel hitherto unreported phenomena.

Rare-earth compounds can be a fertile ground in search for a new frustrated system. The $4f$ elements provide a strong spin-orbit coupling (SOC), which induces large single-ion anisotropy. Its energy scale can be comparable to other interactions such as the dipole interaction and the exchange interaction energy [8,9], leading to competition. The competing interactions with a large SOC that depends on rare-earth elements is the source of various correlated phenomena: spin ice [8], spin liquid [12], metal-insulator transitions [13], and Weyl semimetals [14].

Moreover, the large SOC in rare-earth systems induces $\mathcal{J}$ multiplets as ground states. With a particular crystal electric field (CEF), the states can be further split to make effective $S = 1/2$ [8,15,16] with strong quantum fluctuations. Phenomena like quantum spin ice [17,18] and quantum spin liquid [12,19,20] have been recently reported arising from such strong quantum fluctuations in frustrated systems.

The other important factor is the dimensionality of the system. Low-dimensional structures such as one-dimensional (1D) chains and two-dimensional (2D) triangular lattices, are natural candidates for new interesting ground states. This is because reduced dimensionality prevents the magnetic structure from having a simple collinear configuration and leads to more complicated ground states [21,22]. Equally interesting are the prediction of some exotic phases in three-dimensional (3D) systems [23–25] and the discovery of 3D frustrated materials in pyrochlore and hyperkagome lattices [26–28].

A honeycomb lattice is a bipartite lattice and thus, it is not, *a priori*, frustrated with the nearest neighbor interaction alone. However, it can become frustrated with the addition of further nearest neighbor interactions [29,30]. Only a few inorganic honeycomb systems with large interlayer interaction have been so far reported. $Bi_3Mn_4O_{12}(NO_3)$ with an antiferromagnetic Heisenberg honeycomb bilayer lattice shows frustration due to the competition between the nearest and next-nearest neighbors [31,32]. On the other hand, in $SrLn_2O_4$ (Ln = Gd, Dy, Ho, Er, Tm, and Yb), the zigzag ladders of Ln^{3+} running along the c axis are linked to each other and form a honeycomb lattice on the ab plane [33]. Frustration here leads to an exotic magnetic structure, where both long- and short-range magnetic order coexist at high magnetic field [34,35].

In the previous study of $CuNd_2Ge_2O_8$ [36], it was found that the NdO_8 polyhedra form triangulated dodecahedra. The deviation of the reciprocal susceptibility from the Curie-Weiss law was explained in terms of crystal-field couplings instead of the interaction between Cu^{2+} and Nd^{3+}. The unusual structure based on NdO_8 polyhedra as well as the absence of a long-range order despite the large Curie-Weiss temperature implies significant frustration present in this Nd compound. However, a clear understanding of the microscopic mechanism remains poorly understood. In this study, we have characterized the crystal structure precisely, in particular with respect to the magnetic ions and determined the comprehensive physical properties of several other $CuR_2Ge_2O_8$ materials (R = Pr, Nd, Sm, Eu). These results provide clear evidence of substantial frustration present in these new antiferromagnetic compounds.

II. EXPERIMENTAL METHODS

Single crystals of $CuNd_2Ge_2O_8$ were grown through a self-flux method and several polycrystalline samples of $CuR_2Ge_2O_8$ (R = Pr, Nd, Sm, Eu) were synthesized using a solid state reaction method [36]. To grow the single crystal of $CuNd_2Ge_2O_8$, we used CuO and GeO_2 powder as self-flux

*jgpark10@snu.ac.kr

 ©2017 American Physical Society

and the ratio of the initial materials was CuO : Nd_2O_3 : GeO_2 = 8 : 1 : 6. The mixture was annealed for 30 minutes at 1260 °C in a platinum crucible and then slowly cooled down to 1000 °C at a rate of 2 °C/hour. Using diluted HCl (∼17%) solution, we removed residual flux and byproducts such as CuO and $CuGeO_3$ from the grown crystals. The typical volume of $CuNd_2Ge_2O_8$ single crystals is about 0.001 mm^3 as shown in the photo of one of the crystals in the inset of Fig. 1(a). The color of the crystals is transparent greenish blue and they have an albite shape similar to that reported in Ref. [36].

We also prepared several high-purity polycrystalline samples of $CuR_2Ge_2O_8$ by pelletizing and annealing the mixture of CuO, R_2O_3, and GeO_2 in a stoichiometric ratio, 1 : 1 : 2 for 12 hours at 850 °C. The annealed powder of $CuR_2Ge_2O_8$ was further ground and pelletized before another sintering at elevated temperatures from 950 to 1100 °C at 50 °C steps with a duration of 24 hours at each step. We optimized the final sintering temperature to synthesize the highest-quality samples by carefully monitoring x-ray diffraction (XRD) data.

To check the quality of the samples, we performed high-resolution single-crystal and powder x-ray diffraction experiments. For the full structural refinement of the $CuNd_2Ge_2O_8$ single crystals, we used a XtaLAB P200, Rigaku with a wavelength of 0.710747 Å (a Mo target, averaged K_α). For the structural refinement of polycrystalline $CuR_2Ge_2O_8$ (R = Pr, Nd, Sm, Eu), we used a powder diffractometer (Miniflex II, Rigaku) with wavelengths of 1.540590 and 1.544310 Å ($K_{\alpha1}$ and $K_{\alpha2}$, respectively). The diffraction data were analyzed using the FULLPROF [37] software.

Magnetic and thermodynamic properties of the polycrystalline samples were characterized from 0.4 to 350 K using a MPMS-XL5 and a PPMS-9ECII (Quantum Design) equipped with ^{3}He/^{4}He options. We carried out magnetization measurements up to 140 kOe at 3 K using a PPMS-14 (Quantum Design) with the vibrating sample magnetometer (VSM) option at the National Center for Inter-University Research Facilities (NCIRF) at Seoul National University.

III. EXPERIMENTAL RESULTS AND ANALYSIS

A. Structural analysis

We refined the full crystal structure of $CuNd_2Ge_2O_8$ using a small, high-quality single crystal with the dimensions of 259 × 260 × 88 μm^3 after taking into account the x-ray absorption effects. We collected altogether 2889 Bragg peaks (1860 independent Bragg peaks). The crystal structure was refined using the $I1m1$ unit cell setting of the nonmagnetic rare-earth analog [38]. The unit cell size is a(Å) = 8.342(3), b(Å) = 15.372(4), c(Å) = 5.157(1), β(°) = 89.487(9), and $V(AA^3)$ = 661.2(3). The final results shown in Fig. 1(a) indicate good agreement between the measured data and the refined results. For the structural refinement of other rare-earth cases, we used the data obtained from the powder x-ray diffractometer with the aid of the structural information from the single crystal of $CuNd_2Ge_2O_8$ [see Fig. 1(b)]. The difference between the observed and calculated intensity from the refined structure is small as shown at the bottom of each figure.

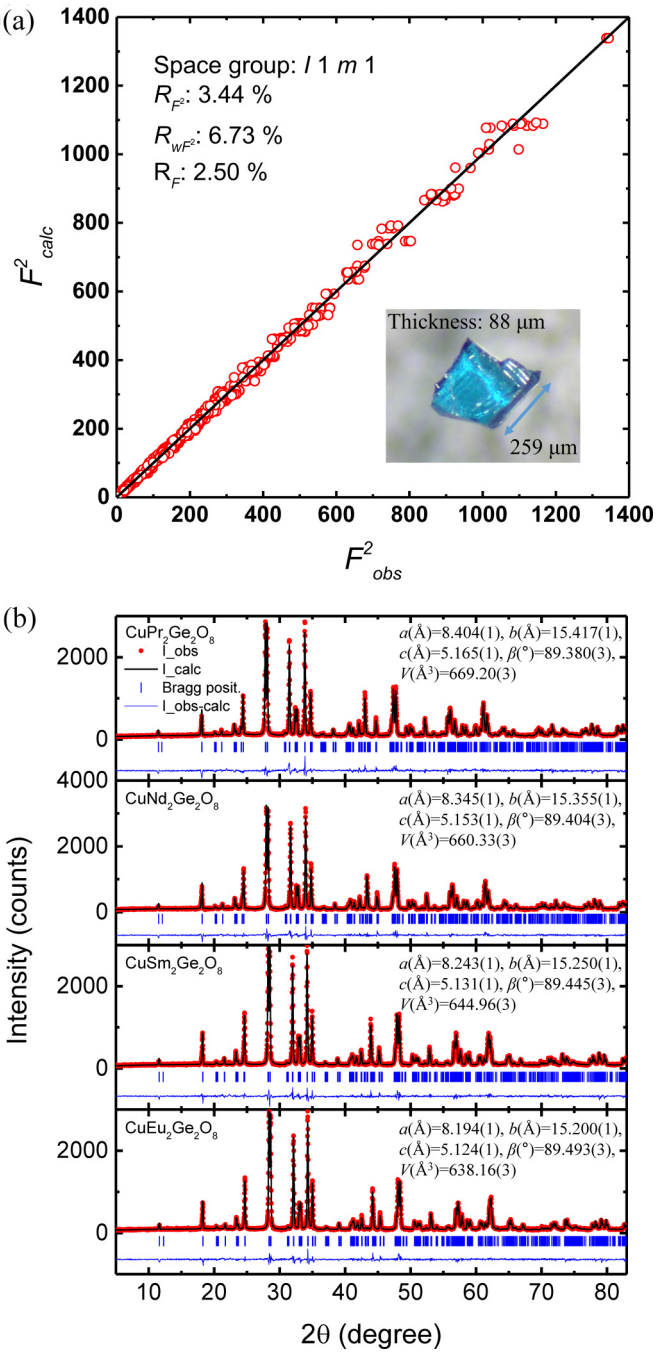

FIG. 1. X-ray diffraction data of $CuR_2Ge_2O_8$ (R = Pr, Nd, Sm, Eu). (a) The refinement result of single-crystal diffraction data of $CuNd_2Ge_2O_8$ and a picture of the single-crystal sample (in the inset). (b) The refinement results of powder diffraction data of $CuR_2Ge_2O_8$. The vertical bars just below the data indicate the position of Bragg peaks. The lines at the bottom represent the difference curves.

Figure 2 shows the refined crystal structure of the $CuNd_2Ge_2O_8$ system, which is isostructural with other rare-earth systems including the nonmagnetic rare-earth analog $Cu(Y/La)_2Ge_2O_8$ [38]. The unit cell size and monoclinic β angle vary depending on the ionic size of R^{3+} [39]. In the previous study of nonmagnetic rare-earth cases [38], the

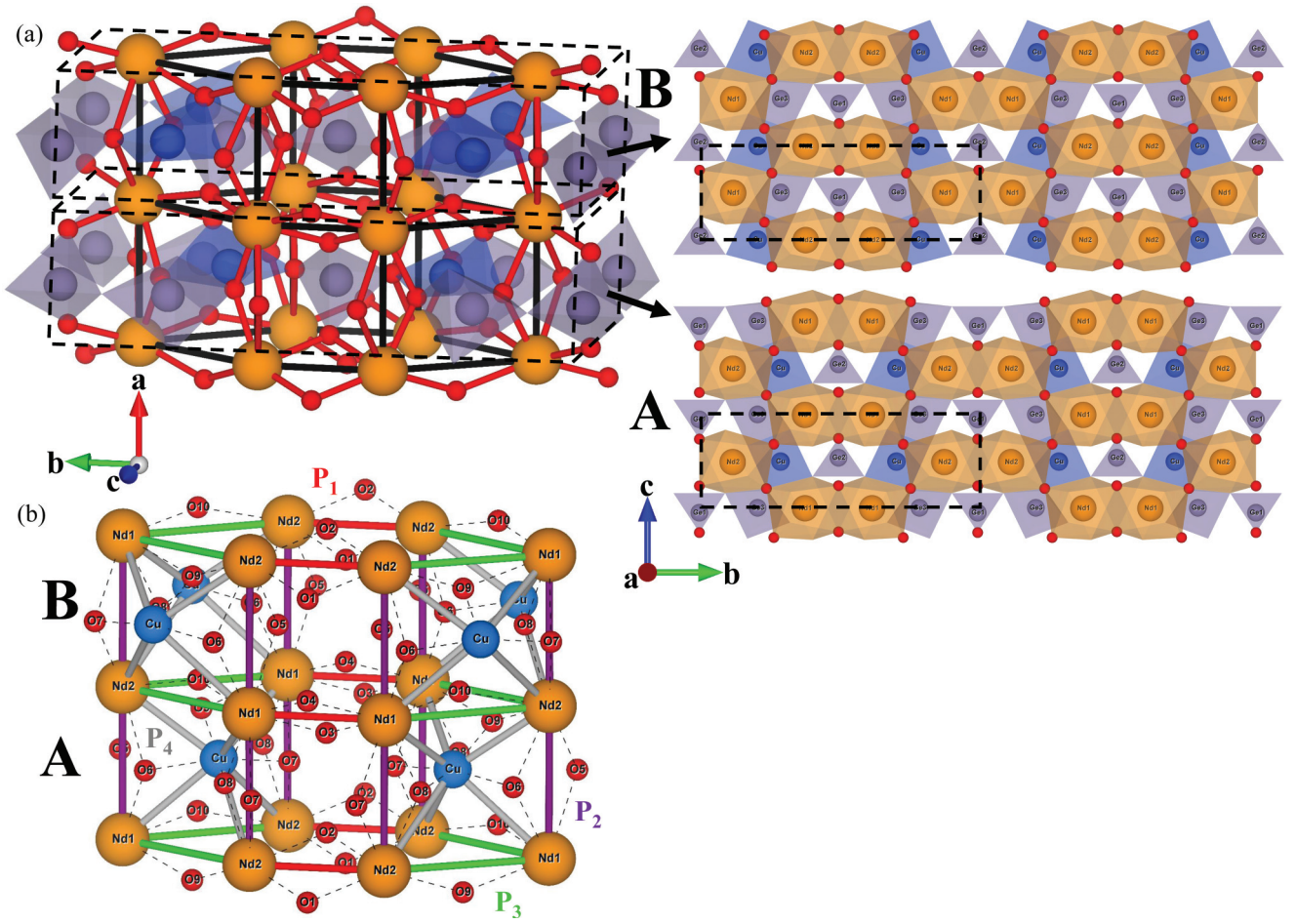

FIG. 2. Crystal structure of $CuNd_2Ge_2O_8$. (a) (Left) The unit cell of $CuNd_2Ge_2O_8$. The orange, blue, gray, and red balls indicate the neodymium, copper, germanium, and oxygen atoms, respectively. We omit some of the oxygen atoms at the corner of the CuO_4 plaquettes, GeO_4 tetrahedra, and GeO_5 bipyramids for simplicity. The red lines display the Nd-O-Nd bond between adjacent Nd atoms, which forms a honeycomb lattice linked along the a axis. (Right) The unit cell can be separated into two sublattices, A and B. The sublattice A contains two copper atoms inside the honeycomb lattice. On the other hand, there are two germanium atoms instead of copper in the sublattice B. (b) The unit cell made of Cu and Nd atoms and the possible exchange paths between the neighboring magnetic atoms: P_1, P_2, P_3, and P_4.

magnetism of the system was characterized by the Cu-ion coordination since Cu is the only magnetic element present in the compound. For magnetic rare-earth cases, however, the magnetism is instead expected to be affected significantly by the large magnetic moments of rare-earth ions.

RO_8 and CuO_4 form distorted triangular dodecahedra and plaquettes, respectively, while germanium oxides have GeO_4 tetrahedra and GeO_5 bipyramids. In the unit cell of $CuNd_2Ge_2O_8$ [see Fig. 2(a) (left)], linked by O atoms, Nd atoms form an elongated honeycomb layer on the bc plane and the layers are linked along the a axis. The unit cell can be separated into two sublattices: A and B. The sublattice A contains two Cu atoms inside the honeycomb. On the other hand, sublattice B contains two Ge atoms inside the honeycomb instead of Cu and the Cu atoms are positioned outside the honeycomb unit [see Fig. 2(a) (right)]. Figure 2(b) shows several exchange paths between adjacent magnetic atoms in the sublattices A and B. The paths P_1 and P_2 are formed by two edge-sharing NdO_8 along the b and a axes, respectively. P_3 follows paths made by two corner-sharing NdO_8 and P_4 indicates the bonding of Nd-O-Cu. The bond lengths and angles of Nd-O-Nd and Nd-O-Cu along each path P_i vary in certain ranges as summarized in Table I.

From the coordination of the R atoms one can immediately see that the magnetic lattice has a honeycomb tunnel-like structure running along the a axis. The interlayer bond length P_2 is comparable to the bond lengths in the honeycomb lattice P_1 and P_3. It suggests that the inter- and intralayer interactions have similar energy scales, which is different from a common 2D honeycomb lattice [40]. Although the bond lengths of P_1, P_2, and P_3 are roughly similar to one another, the bond angles between the magnetic atoms differ significantly from each other. It implies that the sign of exchange interaction along each path is expected to be different as well [41]. Such a complicated mixture of competing interactions is most likely to be a leading factor to make this system frustrated [42–45].

We further note that the structure of $CuR_2Ge_2O_8$ is unique as compared with the previously reported honeycomb systems having an interlayer interaction. For instance, $Bi_3Mn_4O_{12}(NO_3)$ has a honeycomb bilayer lattice made of MnO_6 octahedra with a small anisotropy [31,32] while $SrLn_2O_4$ is governed by dominant interactions on zigzag

TABLE I. Table of bond lengths and angles along each of exchange paths P_i.

	Path	Bond length (Å)	Bond angle (°)
P_1	Nd1-O3-Nd1	4.747(1)	102.6(2)
	Nd1-O4-Nd1	4.685(1)	104.5(3)
	Nd2-O1-Nd2	4.671(1)	104.1(3)
	Nd2-O2-Nd2	4.729(1)	102.3(3)
P_2	Nd1-O5-Nd2	5.495(1)	99.3(2)
	Nd1-O6-Nd2	4.843(1)	119.7(2)
	Nd2-O7-Nd1	5.514(1)	97.7(2)
	Nd2-O8-Nd1	4.735(1)	122.6(2)
P_3	Nd2-O9-Nd1	5.025(1)	141.2(2)
	Nd1-O10-Nd2	4.943(1)	149.2(2)
P_4	Nd1-O6-Cu	4.498(1)	102.6(2)
	Nd2-O6-Cu	4.464(1)	92.4(2)
	Nd1-O7-Cu	4.635(1)	94.2(2)
	Nd2-O7-Cu	4.785(1)	101.8(2)
	Nd1-O8-Cu	4.288(1)	106.6(2)
	Nd2-O8-Cu	4.207(1)	122.2(3)
	Nd1-O9-Cu	4.489(1)	99.0(2)
	Nd2-O9-Cu	4.482(1)	91.4(2)

ladders made of LnO_6 octahedra [33,46]. However, the honeycomb lattice of $CuR_2Ge_2O_8$ is made of RO_8 triangular dodecahedra, which induce different ground states and anisotropy due to the distinct CEF.

B. Magnetic measurements

Figure 3(a) shows the temperature-dependent magnetic susceptibility, $\chi(T)$, of $CuR_2Ge_2O_8$. All the systems show a peak below 5 K, which implies an onset of long-range order. We estimate the ordering temperature from the maximum in the $d\chi/dT$ curve. Figure 3(b) shows the inverse magnetic susceptibility, $1/\chi$. By applying the Curie-Weiss law,

$$\chi(T) = \chi_0 + C/(T - \theta_{CW}), \quad (1)$$

we estimated the temperature-independent term χ_0, effective moments of R^{3+} $\mu_{\text{eff,exp}}$, and the Curie-Weiss temperature θ_{CW} except for the Sm case. The parameters $\mu_{\text{eff,exp}}$ were calculated by the following relation:

$$\mu_{\text{eff,exp}} = \sqrt{\left[3(\mu_{\text{eff,total}})^2 - (\mu_{\text{eff,Cu}})^2\right]/2} \quad (2)$$

(here, $\mu_{\text{eff,total}}$ is the total effective moment from the Curie constant C and $\mu_{\text{eff,Cu}}$ is the effective moment of Cu [38]). For our fitting of the Pr and Nd compounds, we used the data taken above 100 K. The respective ordering temperatures, the experimental and reference effective moments of R^{3+} [47], and the Curie-Weiss temperatures are summarized in Table II.

For the Pr case, χ_0 is estimated to be $\sim 0.8 \times 10^{-3}$ emu/Pr Oe, which is close to Van Vleck paramagnetism due to the crystal electric field effect in $Pr_2Ir_2O_7$ [48]. For the Nd case, we found $\chi_0 \sim 3 \times 10^{-4}$ emu/Nd Oe. The measured effective moments of the Pr and Nd cases ($\mu_{\text{eff,exp,Pr}} = 3.44(2)\mu_B$/Pr and $\mu_{\text{eff,exp,Nd}} = 3.62(3)\mu_B$/Nd) are comparable to the theoretical values of free ion moments, $\mu_{\text{eff,theo}}$. The negative sign of θ_{CW} indicates that the dominant exchange interaction is antiferromagnetic. The ratio of θ_{CW} to the Néel ordering temperature T_N, which is defined as a 'frustration factor' f, is an experimental measure of the strength of frustration [49]. The large value of $f_{Pr} = 12.8$ and $f_{Nd} = 16.2$ indicates that these rare-earth systems are highly frustrated.

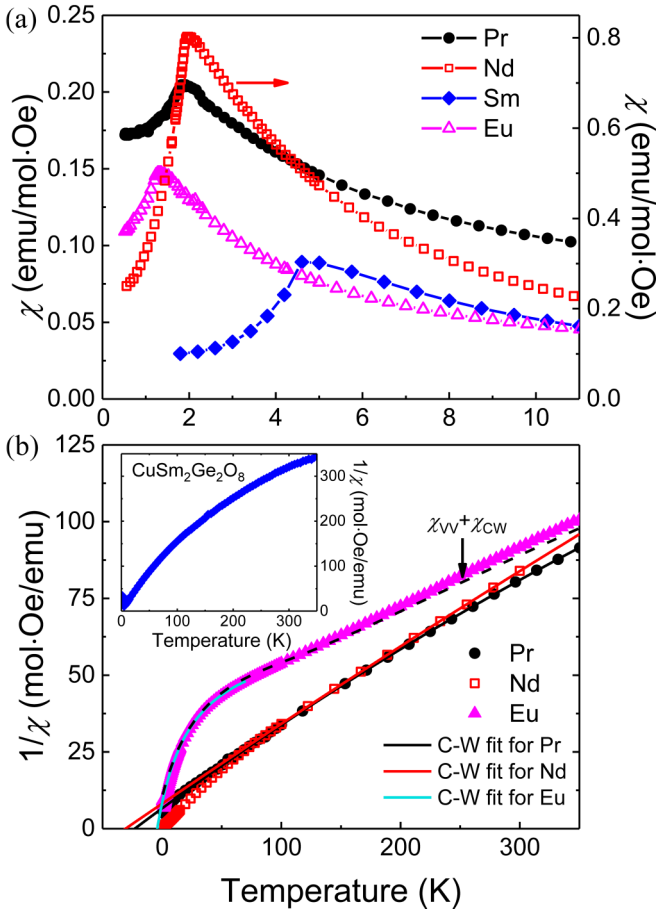

FIG. 3. (a) Temperature-dependent dc magnetic susceptibility $\chi(T)$ of $CuR_2Ge_2O_8$ (R = Pr, Nd, Sm, Eu). (b) The inverse susceptibility curves and the Curie-Weiss (C-W) fitting to the respective data are shown as solid lines. The inset shows the inverse susceptibility of $CuSm_2Ge_2O_8$.

The samarium compound also shows a cusp in $\chi(T)$ at $T_N = 4.34$ K. However, the inverse susceptibility does not follow the Curie-Weiss law due to the intermultiplet splittings with different $\mathcal{J}$ [50,51] and the experimental effective moments around room temperature do not coincide with the theoretical value from Hund's rules [47]. Therefore, we could not estimate the exchange interaction of the ground states from θ_{CW} obtained by fitting the high temperature region. Moreover, the relatively large T_N practically excludes data fitting in the low-temperature region.

For the Eu compound, the fitting was applied on the data taken in the low-temperature region (21 ~ 70 K) due to the low-lying excited states. χ_0 is found to be $\sim 10^{-2}$ emu/mol Oe, which is close to Van Vleck paramagnetism of the nonmagnetic ground state $^7F_0$ of Eu_2O_3 [52]. Also, the effective moment $\mu_{\text{eff,exp,Eu}} = 1.85(2)\mu_B$/mol is close to the effective moment

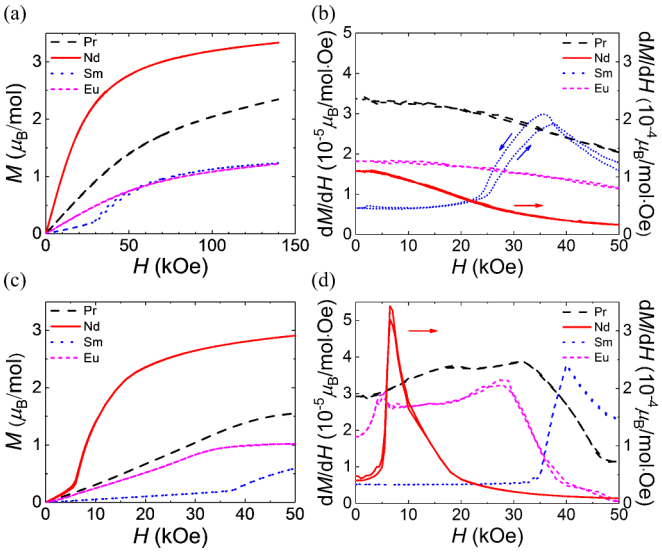

FIG. 4. (a) Field-dependent magnetization $M(H)$ at 3 K and (b) the first derivative $\mathrm{d}M(H)/\mathrm{d}H$ at 3 K. (c) Field-dependent magnetization $M(H)$ measured at 0.6 K below T_N and (d) the first derivative $\mathrm{d}M(H)/\mathrm{d}H$ at 0.6 K.

of Cu^{2+} which suggests that the ground state of the Eu ion in $CuEu_2Ge_2O_8$ is nonmagnetic. To estimate the overall temperature-dependent Van Vleck contribution [the dashed line in Fig. 3(b)], the Cu^{2+} contribution was removed by subtracting the Curie-Weiss term of the La compound [38] from the measured data. The final results ($57 \sim 350$ K) were used for fitting to the Van Vleck paramagnetic susceptibility [53]. The fit provides a spin-orbit coupling constant of $\lambda \sim 423$ K, which is similar to that of the $Eu_2Ir_2O_7$ compound [54]. When we consider just the magnetic moment of Cu^{2+}, the system can be characterized as a two-dimensional triangular antiferromagnet on the ac plane [38]. We note that values of T_N and θ_{CW} are comparable to those of the Y and La cases where $f_Y = 2.2 < f_{Eu} = 3.4 < f_{La} = 6.1$.

To estimate the ground state and anisotropy of all the samples, we measured the field-dependent magnetization $M(H)$. Figures 4(a) and 4(b) present $M(H)$ taken at 3 K up to 140 kOe and its first derivative, respectively. None of the systems show hysteresis around zero field while ramping up and down external magnetic field. Using our high-field magnetization data, we can infer that the moments of the Nd, Sm, and Eu cases are approaching saturation at 140 kOe but the magnetization of the Pr compound increases even at such high magnetic fields. The need for larger external field to saturate Pr moments implies that the single-ion anisotropy and/or exchange interactions between the moments are relatively stronger for the Pr compound than in the other systems.

The saturated magnetization M_s of the Nd case is $\sim 3.3\ \mu_B$/mol. Since there are two Nd^{3+} ions per formula unit, subtracting the Cu contribution $1\ \mu_B$/mol from M_s gives us the Nd contribution equal to $1.15\ \mu_B$/Nd. This value is similar to M_s of $Nd_2Ir_2O_7$ with Ising magnetic anisotropy [55]. The estimated saturation field $H_{\mathrm{sat}} \cong k_B\theta_{CW}/\mu_B g_{\mathcal{J}}\langle\mathcal{J}_z\rangle = 190$ kOe with $\langle\mathcal{J}_z\rangle$ calculated using the ground state of $Nd_2Ir_2O_7$ [56] is also comparable to our experimental results.

For the Sm case, we found $M_s \sim 1.2\ \mu_B$/mol. By excluding the Cu^{2+} moments, magnetization coming from Van Vleck paramagnetism and Sm^{3+} ions is found to have only $0.2\ \mu_B$/mol. Such a small moment of Sm^{3+} is similar to that of a frustrated $Sm_2Ti_2O_7$ system with $\mu_{\mathrm{eff}} = 0.15\ \mu_B$/Sm [50]. On the other hand, M_s of the Eu case is $\sim 1.22\ \mu_B$/mol, which corresponds to the sum of the saturated moment of Cu^{2+} $1\ \mu_B$/mol and the Van Vleck paramagnetism $0.25\ \mu_B$/mol.

Figure 4(c) shows $M(H)$ at 0.6 K for all the systems up to 50 kOe and Fig. 4(d) shows their first derivative $\mathrm{d}M/\mathrm{d}H$ below T_N. All the measured R compounds show a metamagnetic transition below T_N as shown by the $\mathrm{d}M/\mathrm{d}H$ curve. The Pr system reveals two broad humps with a critical field of $H_{c1} = 18$ and $H_{c2} = 32$ kOe in $\mathrm{d}M/\mathrm{d}H$. We note that the critical fields are different from the saturation field. This indicates field-induced phase transitions, which can be related to the phase transition in the spin configuration of Cu^{2+} and Pr^{3+} moments, respectively. The Nd compound shows a sharp peak at $H_c = 6.5$ kOe in $\mathrm{d}M/\mathrm{d}H$. We think this peak is related to an abrupt change in $M(H)$, implying the first-order nature of the transition such as a spin-flop transition. Like the Nd compound, the Sm compound also shows a sharp peak at $H_c = 40$ kOe in $\mathrm{d}M/\mathrm{d}H$.

On the other hand, the Eu compound exhibits a $\mathrm{d}M/\mathrm{d}H$ curve [see Fig. 4(d)] similar to the nonmagnetic rare-earth systems [38], with a peak at $H_c = 5.0$ kOe and the saturation taking place at $H_{\mathrm{sat}} = 29$ kOe. The different behavior of the field-induced transition depending on the rare-earth element indicates that the exchange interactions in the magnetic lattice are significantly affected by the presence of R^{3+}.

C. Heat capacity measurements

Figure 5(a) shows the temperature dependence of heat capacity C_p of $CuR_2Ge_2O_8$ at zero field. A lambdalike sharp peak observed in all four systems below 5 K confirms an onset of the long-range order as observed in $\chi(T)$. The peak position for every measured C_p curve coincides well with T_N extracted from χ within the error bar as shown in Table II. Figure 5(b)

TABLE II. The summary of the magnetic susceptibility data. (*Effective moment of Cu [38].)

	$\mathcal{J}$	T_N(K)	$\frac{\mu_{\mathrm{eff,exp}}}{\mu_B}$	$\frac{\mu_{\mathrm{eff,theo}}}{\mu_B}$	θ_{CW}(K)	$f = \frac{\lvert\theta_{CW}\rvert}{T_N}$
Pr	4	1.80(1)	3.44(2)	3.58	−23.0(7)	12.8(4)
Nd	$\frac{9}{2}$	1.90(1)	3.62(3)	3.62	−31(1)	16.3(5)
Sm	$\frac{5}{2}$	4.3(1)	Undefined	0.85	Undefined	Undefined
Eu	0	1.21(2)	1.85(2)	1.94(1)*	−4.1(3)	3.4(3)

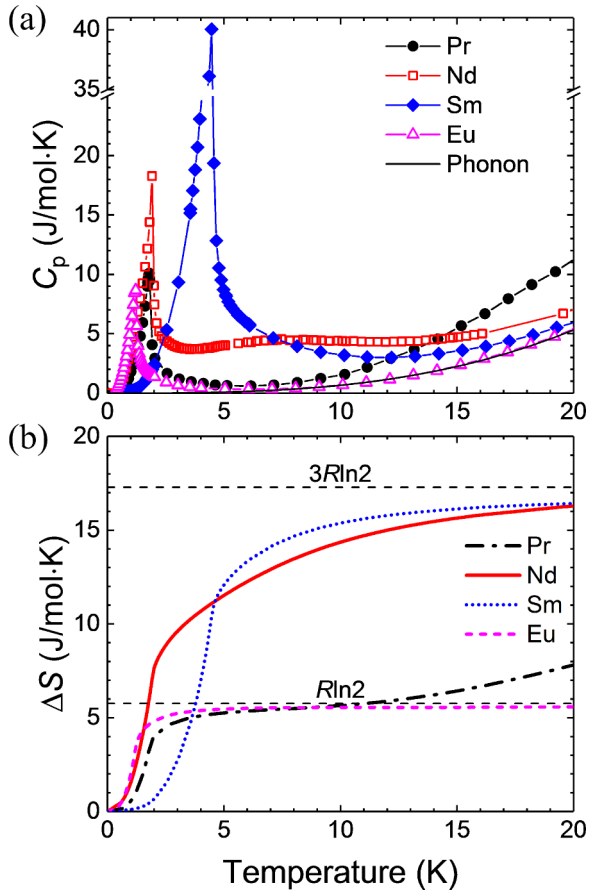

FIG. 5. (a) Heat capacity $C_p(T)$ of $CuR_2Ge_2O_8$ under zero field. The solid line is the phonon contribution of the Eu case estimated by fitting the C_p to the Debye T^3 law. (b) Entropy change ΔS for each R system. The dashed lines stand for the values of $R\ln 2$ and $3R\ln 2$, respectively.

plots the entropy change ΔS of each case. The phonon contribution C_{phonon} of the Eu compound was evaluated using the Debye T^3 law in the low-temperature region ($T < 20$ K). The C_{phonon} contribution of the other magnetic R compounds was estimated by scaling the C_{phonon} of Eu [57].

For the Eu case, since the spin degree of freedom comes mainly from Cu^{2+} $S = 1/2$ (as shown by the magnetization measurements), the entropy change saturates at $R\ln 2 = 5.76\,\text{J/mol K}$. At $T_N = 1.21$ K, however, the entropy change ΔS_{Eu} is $\sim 3.39\,\text{J/mol K}$, which corresponds to 59% of $R\ln 2$. The residual entropy released above T_N originates from the correlation that remains short-ranged due to the geometrical frustration of the 2D triangular lattice [58,59].

In $CuPr_2Ge_2O_8$, the Pr^{3+} ground state can be either a non-Kramers doublet or a nonmagnetic singlet [48,60]. Given the value of μ_{eff} and the significant difference in $M(H)$ between Pr and nonmagnetic rare-earth Eu cases, the ground state of Pr ions in $CuPr_2Ge_2O_8$ is likely to be the magnetic non-Kramers doublet. In such a case, the total entropy is expected to reach $3R\ln 2$ at high temperature including the Cu contribution of $R\ln 2$. However, the actual entropy obtained at T_N is ΔS_{Pr} is ~ 3.35 J/mol K at $T_N = 1.8$ K, which is only 19% of $3R\ln 2$ as shown in Fig. 5(b). Such a reduction of entropy indicates that the spin moments of Pr are highly frustrated similar to the frustrated pyrochlore system $Ln_2Ir_2O_7$ [61]. The residual entropy is released well above $T > |\theta_{CW}|$ eventually reaching $3R\ln 2$ at high temperature. The difference between C_p and C_{phonon} above T_N shows the short-range ordering of the Pr magnetic moments.

In the case of the $CuNd_2Ge_2O_8$ compound, magnetism at T_N mainly comes from the ground state of the Kramers doublet of Nd; the excited states do not contribute due to the large CEF splittings between the ground and excited states [56]. Therefore, the total entropy change is expected to approach the value of $3R\ln 2$ including Cu contribution, consistent with our data in Fig. 5(b). At $T_N = 1.90$ K, $\Delta S_{Nd} \sim 7.04\,\text{J/mol K}$ which corresponds to $0.41 \times 3R\ln 2$. Such a small entropy fraction below T_N and large residual entropy above T_N with a broad hump in C_p reflects short-range order in this frustrated system.

For the Sm compound, we observe a tail above T_N which is a typical sign of short-range order of frustrated systems in the specific heat. Similar to the Nd compound, the ground state of Sm^{3+} is a Kramers doublet. Again, the respective value of $\Delta S_{Sm} \sim 10.37\,\text{J/mol K}$ is observed as shown in Fig. 5(b) at $T_N = 4.3$ K. The entropy difference reaches $0.60 \times 3R\ln 2$. This small entropy fraction and the large residual entropy above T_N is also linked to short-range interactions in this frustrated system.

IV. DISCUSSION

$CuR_2Ge_2O_8$ (R = Pr, Nd, Sm, Eu) compounds are candidates for a new frustrated system of rare-earth magnetism. For the Eu case, physical quantities such as μ_{eff}, M_s, and ΔS show that the ground state of Eu^{3+} is nonmagnetic. Therefore $CuEu_2Ge_2O_8$ is a 2D triangular antiferromagnet with Cu^{2+} $S = 1/2$ quantum spins lying on the ac plane. The triangular plane corrugates in a zigzag shape along the a axis [38]. The Néel temperature of the Eu compound is comparable to $T_{N,Y} = 0.51$ and $T_{N,La} = 1.09$ K.

In the case of the Pr and Nd compounds, there is an anomaly in $\chi(T)$ around T_N. Above $T > T_N$, it follows paramagnetic behavior with a relatively small temperature-independent Van Vleck paramagnetic term related to large crystal-field splittings from the ground state to higher excited states. The small Van Vleck term suggests that θ_{CW} is mainly contributed by the exchange interactions and not by CEF [48]. For a low-dimensional magnetic system, one would expect a broad hump [62–66] at $\sim|\theta_{CW,Pr}| = 23$ K and $|\theta_{CW,Nd}| = 31$ K. Absence of this feature supports the 3D antiferromagnetic scenario in these systems rather than 1D or 2D.

The large frustration factors $f_{Pr} = 12.8$ and $f_{Nd} = 16.3$ obtained from our magnetic susceptibility data point to the substantial frustration in these two systems. The results of the thermodynamic measurements support the significant frustration scenario as well. Similar to other frustrated systems [67,68], the entropy change does not reach $3R\ln 2$ corresponding to the spin degree of freedom of the ground state below T_N. The broad hump in the C_p curve signals that the residual entropy is released above T_N. This is quite different from an unfrustrated system, which releases the majority of its entropy below the ordering temperature [57]. The hump in

C_p for a rare-earth system might also be explained by the Schottky anomaly due to the splittings of the ground state $\mathcal{J}$ manifold [69]. In this case, the temperature scale of the anomaly is expected to be comparable to the energy level splittings. We note that the small Van Vleck paramagnetism of the Pr and Nd cases implies that the spitting is in the order of 100 K considering the similar RO_8 dodecahedra of $R_2X_2O_7$ (X = Ir,Sn) [48,56,70]. However, the Nd compound shows the broad hump in $C_p - C_{\text{phonon}}$ at temperatures well below 100 K, which indicates that the hump originates from frustration rather than a Schottky anomaly.

Along with other R compounds, the Sm case is also a candidate material for a 3D frustrated system. Like Pr and Nd cases, the absence of a broad hump in $\chi(T)$ indicates 3D magnetic lattice. Even though we cannot determine the frustration factor, the thermodynamic measurement shows the presence of frustrated moments. For example, the tail in $C_p - C_{\text{phonon}}$ above T_N appears due to a short-range correlation even surviving at high temperatures. The large fraction of entropy change released above T_N shows a sign of short-range order.

The magnitude of T_N for the Pr case is around 1 K, which is comparable to T_N of their nonmagnetic rare-earth counterparts (the Eu compound in Fig. 5 and the Y/La compounds in [38]). Moreover, the entropy contribution from the sharp peak is similar to the entropy contribution of Cu^{2+} $R\ln 2$ rather than $3R\ln 2$. These aspects suggest that only Cu^{2+} moments order while the R^{3+} moments do not. Nevertheless, this issue cannot be resolved without the help of neutron diffraction which is left for a future study.

V. CONCLUSION

We have synthesized a single crystal of $CuNd_2Ge_2O_8$ and several polycrystalline samples of $CuR_2Ge_2O_8$ (R = Pr, Nd, Sm, Eu), analyzed their crystal structure, and characterized their magnetic and thermodynamic properties. While the ground state of the Eu compound is driven solely by the Cu ions, the Pr, Nd, and Sm compounds show a 3D honeycomb-tunnel-like lattice made of R^{3+}. They display a large frustration factor, a small fraction of the entropy released at T_N ($19 \sim 60\%$ of $3R\ln 2$), and short-range order above T_N, characteristic behavior of a frustrated antiferromagnet. Frustration in $CuR_2Ge_2O_8$ is induced by the interplay of crystal structure providing a route to bring in competing interactions and the anisotropy from the large spin-orbit coupling of the rare-earth elements.

ACKNOWLEDGMENTS

We thank Santu Baidya, Choong Hyun Kim, Darren Peets, and Yukio Noda for discussion. We also acknowledge Kohki Satoh from Quantum Design Japan Inc. and Young-Mi Song from NCIRF for their help with some of the measurements. The work at the IBS CCES was supported by the Institute for Basic Science in Korea (IBS-R009-G1).

[1] M. F. Collins and O. A. Petrenko, Can. J. Phys. **75**, 605 (1997).
[2] R. Moessner, Can. J. Phys. **79**, 1283 (2001).
[3] M. Pregelj, A. Zorko, O. Zaharko, H. Nojiri, H. Berger, L. C. Chapon, and D. Arčon, Nat. Commun. **6**, 7255 (2015).
[4] R. Nath, Y. Furukawa, F. Borsa, E. E. Kaul, M. Baenitz, C. Geibel, and D. C. Johnston, Phys. Rev. B **80**, 214430 (2009).
[5] M. Hälg, W. E. A. Lorenz, K. Yu. Povarov, M. Månsson, Y. Skourski, and A. Zheludev, Phys. Rev. B **90**, 174413 (2014).
[6] W. Jin and O. A. Starykh, J. Phys.: Conf. Ser. **828**, 012019 (2017).
[7] J.-H. Chung, Y. S. Song, S. Park, H. Ueda, Y. Ueda, and S.-H. Lee, J. Korean Phys. Soc. **62**, 1900 (2013).
[8] A. P. Ramirez, A. Hayashi, R. J. Cava, R. Siddharthan, and B. S. Shastry, Nature (London) **399**, 333 (1999).
[9] S. V. Isakov, R. Moessner, and S. L. Sondhi, Phys. Rev. Lett. **95**, 217201 (2005).
[10] H. Kawamura and S. Miyashita, J. Phys. Soc. Jpn. **54**, 4530 (1985).
[11] Y. Shirata, H. Tanaka, A. Matsuo, and K. Kindo, Phys. Rev. Lett. **108**, 057205 (2012).
[12] J. S. Gardner, B. D. Gaulin, A. J. Berlinsky, P. Waldron, S. R. Dunsiger, N. P. Raju, and J. E. Greedan, Phys. Rev. B **64**, 224416 (2001).
[13] K. Ueda, J. Fujioka, and Y. Tokura, Phys. Rev. B **93**, 245120 (2016).
[14] E. Y. Ma, Y.-T. Cui, K. Ueda, S. Tang, K. Chen, N. Tamura, P. M. Wu, J. Fujioka, Y. Tokura, and Z.-X. Shen, Science **350**, 538 (2015).
[15] Y. M. Jana, A. Sengupta, and D. Ghosh, J. Magn. Magn. Mater. **248**, 7 (2002).
[16] S. H. Curnoe, Phys. Rev. B **88**, 014429 (2013).
[17] LiDong Pan, N. J. Laurita, Kate A. Ross, Bruce D. Gaulin, and N. P. Armitage, Nat. Phys. **12**, 361 (2016).
[18] K. Kimura, S. Nakatsuji, J-J. Wen, C. Broholm, M. B. Stone, E. Nishibori, and H. Sawa, Nat. Commun. **4**, 1934 (2013).
[19] H. Takatsu, H. Kadowaki, T. J. Sato, J. W. Lynn, Y. Tabata, T. Yamazaki, and K. Matsuhira, J. Phys.: Condens. Matter **24**, 052201 (2012).
[20] Y. Tokiwa, J. J. Ishikawa, S. Nakatsuji, and P. Gegenwart, Nat. Mater. **13**, 356 (2014).
[21] N. D. Mermin and H. Wagner, Phys. Rev. Lett. **17**, 1133 (1966).
[22] P. W. Anderson, Mater. Res. Bull. **8**, 153 (1973).
[23] M. Hermele, M. P. A. Fisher, and L. Balents, Phys. Rev. B **69**, 064404 (2004).
[24] A. Banerjee, Sergei V. Isakov, K. Damle, and Y. B. Kim, Phys. Rev. Lett. **100**, 047208 (2008).
[25] O. Sikora, F. Pollmann, N. Shannon, K. Penc, and P. Fulde, Phys. Rev. Lett. **103**, 247001 (2009).
[26] Y. Okamoto, M. Nohara, H. Aruga-Katori, and H. Takagi, Phys. Rev. Lett. **99**, 137207 (2007).
[27] M. J. Lawler, H.-Y. Kee, Y. B. Kim, and A. Vishwanath, Phys. Rev. Lett. **100**, 227201 (2008).
[28] P. Khuntia, F. Bert, P. Mendels, B. Koteswararao, A. V. Mahajan, M. Baenitz, F. C. Chou, C. Baines, A. Amato, and Y. Furukawa, Phys. Rev. Lett. **116**, 107203 (2016).

[29] R. F. Bishop, P. H. Y. Li, O. Götze, J. Richter, and C. E. Campbell, Phys. Rev. B **92**, 224434 (2015).
[30] J. Rehn, Arnab Sen, Kedar Damle, and R. Moessner, Phys. Rev. Lett. **117**, 167201 (2016).
[31] O. Smirnova, M. Azuma, N. Kumada, Y. Kusano, M. Matsuda, Y. Shimakawa, T. Takei, Y. Yonesaki, and N. Kinomura, J. Am. Chem. Soc. **131**, 8313 (2009).
[32] H. C. Kandpal and J. van den Brink, Phys. Rev. B **83**, 140412(R) (2011).
[33] H. Karunadasa, Q. Huang, B. G. Ueland, J. W. Lynn, P. Schiffer, K. A. Regan, and R. J. Cava, Phys. Rev. B **71**, 144414 (2005).
[34] T. J. Hayes, G. Balakrishnan, P. P. Deen, P. Manuel, L. C. Chapon, and O. A. Petrenko, Phys. Rev. B **84**, 174435 (2011).
[35] D. L. Quintero-Castro, B. Lake, M. Reehuis, A. Niazi, H. Ryll, A. T. M. N. Islam, T. Fennell, S. A. J. Kimber, B. Klemke, J. Ollivier, V. Garcia Sakai, P. P. Deen, and H. Mutka, Phys. Rev. B **86**, 064203 (2012).
[36] J. Campá, E. Gutiérrez-Puebla, M. Monge, C. Valero, J. Mira, J. Rivas, C. Cascales, and I. Rasines, J. Solid State Chem. **120**, 254 (1995).
[37] J. Rodriguez-Carvajal, Physica B **192**, 55 (1993).
[38] H. Cho, M. Kratochvílová, H. Sim, K.-Y. Choi, C. H. Kim, C. Paulsen, M. Avdeev, D. C. Peets, Y. Jo, S. Lee, Y. Noda, M. J. Lawler, and J.-G. Park, Phys. Rev. B **95**, 144404 (2017).
[39] U. Lambert and W. Eysel, Powder Diffr. **1**, 256 (1986).
[40] T. J. Sato, S.-H. Lee, T. Katsufuji, M. Masaki, S. Park, J. R. D. Copley, and H. Takagi, Phys. Rev. B **68**, 014432 (2003).
[41] J. Goodenough, *Magnetism and the Chemical Bond* (Interscience, New York, 1963).
[42] C. Balz, B. Lake, J. Reuther, H. Luetkens, R. Schönemann, T. Herrmannsdörfer, Y. Singh, A. T. M. Nazmul Islam, E. M. Wheeler, J. A. Rodriguez-Rivera, T. Guidi, G. G. Simeoni, C. Baines, and H. Ryll, Nat. Phys. **12**, 942 (2016).
[43] S. Derakhshan, J. E. Greedan, T. Katsumata, and L. M. D. Cranswick, Chem. Mater. **20**, 5714 (2008).
[44] R. Nirmala, K.-H. Jang, H. Sim, H. Cho, J. Lee, N.-G. Yang, S. Lee, R. M. Ibberson, K. Kakurai, M. Matsudau, S.-W. Cheong, V. V. Gapontsev, S. V. Streltsov, and J.-G. Park, J. Phys.: Condens. Matter. **29**, 13LT01 (2017).
[45] D. C. Peets, H. Sim, S. Choi, M. Avdeev, S. Lee, S. J. Kim, H. Kang, D. Ahn, and J.-G. Park, Phys. Rev. B **95**, 014424 (2017).
[46] J.-J. Wen, W. Tian, V. O. Garlea, S. M. Koohpayeh, T. M. McQueen, H.-F. Li, J.-Q. Yan, J. A. Rodriguez-Rivera, D. Vaknin, and C. L. Broholm, Phys. Rev. B **91**, 054424 (2015).
[47] S. Blundell, *Magnetism in Condensed Matter* (Oxford University Press, New York, 2001).
[48] S. Nakatsuji, Y. Machida, Y. Maeno, T. Tayama, T. Sakakibara, J. van Duijn, L. Balicas, J. N. Millican, R. T. Macaluso, and Julia Y. Chan, Phys. Rev. Lett. **96**, 087204 (2006).
[49] A. Ramirez, Annu. Rev. Mater. Sci. **24**, 453 (1994).
[50] S. Singh, S. Saha, S. K. Dhar, R. Suryanarayanan, A. K. Sood, and A. Revcolevschi, Phys. Rev. B **77**, 054408 (2008).
[51] J. Pospíšil, M. Kratochvílová, J. Prokleška, M. Diviš, and V. Sechovský, Phys. Rev. B **81**, 024413 (2010).
[52] A. S. Borovik-Romanov and N. M. Kreines, Sov. Phys. JETP **2**, 4 (1956).
[53] Y. Takikawa, S. Ebisu, and S. Nagata, J. Phys. Chem. Solids **71**, 1592 (2010).
[54] J. J. Ishikawa, E. C. T. O'Farrell, and S. Nakatsuji, Phys. Rev. B **85**, 245109 (2012).
[55] Z. Tian, Y. Kohama, T. Tomita, H. Ishizuka, T. H. Hsieh, J. J. Ishikawa, K. Kindo, L. Balents, and S. Nakatsuji, Nat. Phys. **12**, 134 (2016).
[56] M. Watahiki, K. Tomiyasu, K. Matsuhira, K. Iwasa, M. Yokoyama, S. Takagi, M. Wakeshima, and Y. Hinatsu, J. Phys. Conf. Ser. **320**, 012080 (2011).
[57] V. Goruganti, K. D. D. Rathnayaka, Joseph H. Ross, Jr., Y. Öner, C. S. Lue, and Y. K. Kuo, J. Appl. Phys. **103**, 073919 (2008).
[58] K. Yokota, N. Kurita, and H. Tanaka, Phys. Rev. B **90**, 014403 (2014).
[59] J. Park, S. Lee, M. Kang, K.-H. Jang, C. Lee, S. V. Streltsov, V. V. Mazurenko, M. V. Valentyuk, J. E. Medvedeva, T. Kamiyama, and J.-G. Park, Phys. Rev. B **82**, 054428 (2010).
[60] A. J. Princep, D. Prabhakaran, A. T. Boothroyd, and D. T. Adroja, Phys. Rev. B **88**, 104421 (2013)
[61] K. Matsuhira, M. Wakeshima, Y. Hinatsu, and S. Takagi, J. Phys. Soc. Jpn. **80**, 094701 (2011).
[62] J. Bonner and M. Fisher, Phys. Rev. **135**, A640 (1964).
[63] M. Hase, I. Terasaki, and K. Uchinokura, Phys. Rev. Lett. **70**, 3651 (1993).
[64] B. Koteswararao, S. Salunke, A. V. Mahajan, I. Dasgupta, and J. Bobroff, Phys. Rev. B **76**, 052402 (2007).
[65] N. Kini, E. Kaul, and C. Geibel, J. Phys.: Condens. Matter **18**, 1303 (2006).
[66] N. Elstner, R. R. P. Singh, and A. P. Young, Phys. Rev. Lett. **71**, 1629 (1993).
[67] T. Radu, H. Wilhelm, V. Yushankhai, D. Kovrizhin, R. Coldea, Z. Tylczynski, T. Lühmann, and F. Steglich, Phys. Rev. Lett. **95**, 127202 (2005).
[68] B. Canals, I.-A. Chioar, V.-D. Nguyen, M. Hehn, D. Lacour, F. Montaigne, A. Locatelli, T. O. Menteş, B. S. Burgos, and N. Rougemaille, Nat. Commun. **7**, 11446 (2016).
[69] E. S. R. Gopal, *Specific Heats at Low Temperatures* (Plenum Press, New York, 1966).
[70] H. D. Zhou, C. R. Wiebe, J. A. Janik, L. Balicas, Y. J. Yo, Y. Qiu, J. R. D. Copley, and J. S. Gardner, Phys. Rev. Lett. **101**, 227204 (2008).